A Short Mean Free Path at $z = 6$ Favors Late and Rapid Reionization by Faint Galaxies

Christopher Cain , Anson D'Aloisio, Nakul Gangolli, and George D. Becker
Department of Physics and Astronomy, University of California, Riverside, CA 92521, USA; ccain002@ucr.edu
Received 2021 May 25; revised 2021 July 14; accepted 2021 August 3; published 2021 August 24

Abstract

Recent measurements of the ionizing photon mean free path ($\lambda_{912}^{\rm mfp}$) at $5 < z < 6$ suggest that the IGM was rapidly evolving at those times. We use radiative transfer simulations to explore the implications for reionization, with a focus on the short value of $\lambda_{912}^{\rm mfp} = 3.57_{-2.14}^{+3.09}$ cMpc h^{-1} at $z = 6$. We introduce a model for subresolution ionizing photon sinks based on radiative hydrodynamics simulations of small-scale IGM clumping. We argue that the rapid evolution in $\lambda_{912}^{\rm mfp}$ at $z = 5 - 6$, together with constraints on the metagalactic ionizing background, favors a late reionization process in which the neutral fraction evolved rapidly in the latter half. We also argue that the short $\lambda_{912}^{\rm mfp}(z = 6)$ points to faint galaxies as the primary drivers of reionizaton. Our preferred model, with $\lambda_{912}^{\rm mfp}(z = 6) = 6.5$ Mpc h^{-1}, has a midpoint of $z = 7.1$ and ends at $z = 5.1$. It requires three ionizing photons per H atom to complete reionization and a LyC photon production efficiency of $\log(f_{\rm esc}^{\rm eff}\,\xi_{\rm ion}/[\rm erg^{-1}Hz]) = 24.8$ at $z > 6$. Recovering $\lambda_{912}^{\rm mfp}(z = 6)$ as low as the measured central value may require an increase in IGM clumpiness beyond predictions from simulations, with a commensurate increase in the photon budget.

Unified Astronomy Thesaurus concepts: Cosmology (343); Galaxy formation (595); Early universe (435); Reionization (1383)

1. Introduction

There are several lines of evidence that reionization ended around $z = 6$, or perhaps later. The large Lyα forest opacity fluctuations at $z \geqslant 5.5$ have been attributed to neutral islands below $z = 6$ (Becker et al. 2015; Bosman et al. 2018; Eilers et al. 2018; Keating et al. 2020b; Kulkarni et al. 2019; Nasir & D'Aloisio 2020; Qin et al. 2021). Other independent constraints from high-z Lyα emitter (LAE) surveys and quasar damping wing analyses also suggest a significantly neutral IGM at $z \sim 7$ (Kashikawa et al. 2006; Davies et al. 2018; Wang et al. 2020; Ono et al. 2011; Schenker et al. 2012; Pentericci et al. 2014). The reionization models invoked to explain these observations are consistent with the low value of cosmic microwave background optical depth reported by Planck, $\tau_{\rm CMB} = 0.054 \pm 0.007$ (Planck Collaboration et al. 2020). Given large uncertainties in these measurements, however, it is unclear whether reionization was rapid or more extended in duration (e.g., Finkelstein et al. 2019). In this Letter, we argue that recent measurements of the mean free path at $5 < z \leqslant 6$ point to a reionization process that was both late and rapid.

The new evidence considered here was reported by Becker et al. (2021, B21). They extended direct measurements of the mean free path (MFP; $\lambda_{912}^{\rm mfp}$) to $z = 6$ and found a rather low value of $\lambda_{912}^{\rm mfp}(z = 6) = 3.57_{-2.14}^{+3.09}$ cMpc h^{-1}. This disfavors at the 97% level even the low MFP predicted by the "Low $\tau_{\rm CMB}$" model of Keating et al. (2020a), in which the IGM was still 20% neutral at $z = 6$ and reionization ended at $z \approx 5.3$. The B21 result suggests that ionizing photon sinks played a larger role than previous models have captured, and/or that the IGM was even more neutral at $z = 6$.

Recent theoretical work has demonstrated that modeling the sinks is complicated by the interplay between self-shielding and the hydrodynamic response of the IGM to photoheating (Park et al. 2016; D'Aloisio et al. 2020). Before reionization, the gas clumps down to its Jeans scale, which in the ΛCDM cosmology can be as low as $\sim$1 kpc. After ionization fronts

(I-fronts) sweep through, the local density structure "relaxes" by Jeans smoothing and photoevaporative processes, evolving to a less clumpy state over a timescale $\Delta t \sim 200$ Myr. State-of-the-art radiative hydrodynamics (RHD) simulations have yet to fully bridge the scale gap between the sinks and the $\gtrsim 100$ Mpc boxes necessary to converge on reionization observables (Iliev et al. 2014). In addition, the largest dynamic ranges have been achieved with moment-based radiative transfer (RT) methods, which may be numerically inaccurate in the sinks (Wu et al. 2021).

A key addition of this work is that we have developed a new subgrid model for the sinks based on the study of D'Aloisio et al. (2020, D20). We have incorporated this into a new ray tracing RT code, giving our reionization simulations a formal dynamic range of over 5 orders of magnitude in scale. In this Letter, we present first results from this new simulation framework and we use them to interpret the B21 measurements.

This Letter is organized as follows. In Section 2, we describe our numerical methods. In Section 3 we present our results and we conclude in Section 4.

2. Numerical Methodology

We ran RT simulations of reionization in a $(200h^{-1}$ c Mpc$)^3$ volume using our new ray tracing code, which we will describe in detail elsewhere (C. Cain & A. D'Aloisio, 2021 in preparation). We use a coarse-grained uniform RT grid with $N = 200^3$. The premise is to use a pre-run suite of highly resolved (small volume) RHD simulations to model the opacity evolution in each $(1\ h^{-1}\,\rm Mpc)^3$ RT cell during reionization.

2.1. Coarse-grained RT

Our monochromatic RT algorithm traces rays from source cells using an adaptive splitting and merging scheme based on Abel & Wandelt (2002) and similar to the procedure of Trac & Cen (2007). We track 48 directions (HEALPix level 1) and use the full speed of light because the commonly adopted reduced-speed approximation leads to inaccuracies near the end

of reionization. We propagate subgrid "moving-screen" I-fronts across the coarse cells with speed $v_{IF} = \frac{F}{(1+\chi)n_H}$, where F is the incident ionizing flux, n_H is the proper H density, and $\chi = n_{He}/n_H \approx 0.082$ accounts for singly ionized helium. We assume that ray j intersecting cell i contributes photoionizations over a path length $x_{ion}^i \Delta s^{ij}$, where x_{ion}^i is the cell ionized fraction and Δs^{ij} is the total path length of the ray through the cell. We further assume that the MFP in the ionized part of the cell takes a locally uniform value, $\overline{\lambda}^i$. The mean H photoionization rate there is

$$\Gamma_{HI}^i = \sum_{j=1}^{N_{rays}} \frac{N_{\gamma,0}^{ij}[1 - \exp(-x_{ion}^i \Delta s^{ij}/\overline{\lambda}^i)] \big/ \Delta t}{x_{ion}^i V_{cell} \big/ \overline{\sigma}_{HI}\overline{\lambda}^i}, \quad (1)$$

where $N_{\gamma,0}^{ij}$ is the number of photons incident on the cell in a time Δt from ray j, V_{cell} is the cell volume, and $\overline{\sigma}_{HI}$ is the H photoionization cross-section. The over-bars denote frequency averages. To compute these quantities, we assume a specific intensity of $J_\nu \propto \nu^{-1.5}$ between 1 and 4 Ry, consistent with models of young metal-poor stellar populations (e.g., D'Aloisio et al. 2019). The numerator of Equation (1) counts H ionizations per unit time. The denominator gives the number of H I atoms in ionized gas since $(\overline{\sigma}_{HI}\overline{\lambda}^i)^{-1}$ is the Γ_{HI}-weighted mean n_{HI}. We tested this moving-screen framework against simulations of plane-parallel I-fronts similar to those in D20 (but with one domain) and found good agreement in the photon budget. For comparison against Lyα forest measurements, we track temperatures on the RT grid using the approximate method of D'Aloisio et al. (2019). We adopt their fit for the post I-front temperature, T_{reion}, and the subsequent thermal evolution is modeled using their Equation (6).

2.2. Subgrid Model for $\overline{\lambda}$

We extract $\overline{\lambda}$ from the RHD simulations of D20, which use $N_{dm} = N_{gas} = N_{rt} = 1024^3$ dark matter particles and gas/RT cells in a $(1\,h^{-1}\,Mpc)^3$ box. These simulations are parameterized by three environmental quantities: the reionization redshift, z_{re}, the impinging Γ_{HI}, which quantifies the strength of the external ionizing background, and the box-scale linear overdensity over its standard deviation, δ/σ. We have expanded the D20 suite to include all combinations of $\Gamma_{-12} \equiv \Gamma_{HI}/10^{-12}\,s^{-1} \in \{0.03, 0.3, 3.0\}$, $z_{re} \in \{12, 8, 6\}$, and $\delta/\sigma \in \{-\sqrt{3}, 0, \sqrt{3}\}$. For cells reionized below $z_{re} = 6$, we extrapolate logarithmically in cosmic time. We tested our extrapolation against a simulation with $z_{re} = 5.2$ and found good agreement. The frequency-averaged MFP is obtained using $\overline{\lambda}^{-1} = \langle n_{HI}\Gamma_{HI}\rangle_V / F$, where $\langle \ldots \rangle_V$ is a volume average.

The D20 simulations track the self-shielding and hydrodynamic response of the IGM in the wake of I-fronts sourced by a steady background (constant Γ_{HI}). However, Γ_{HI} can evolve considerably in realistic environments. Using D20-style simulations with time-varying Γ_{HI}, we have developed an empirical model for the evolution of $\overline{\lambda}$,

$$\frac{d\overline{\lambda}}{dt} = \left.\frac{\partial\overline{\lambda}}{\partial t}\right|_{\Gamma_{HI}} + \left.\frac{\partial\overline{\lambda}}{\partial\Gamma_{HI}}\right|_t \frac{d\Gamma_{HI}}{dt} - \frac{\overline{\lambda} - \overline{\lambda}_{eq}}{t_{relax}}. \quad (2)$$

The first term on the right is the quantity measured from the D20 simulations—the evolution of $\overline{\lambda}$ at fixed Γ_{HI}. The second term captures the instantaneous change in $\overline{\lambda}$ with Γ_{HI}. The last term implements a relaxation timescale t_{relax} over which $\overline{\lambda}$

evolves toward an equilibrium value $\overline{\lambda}_{eq}$ in response to a sudden increase in Γ_{HI}. The $\left.\frac{\partial\overline{\lambda}}{\partial t}\right|_{\Gamma_{HI}}$ term and $\overline{\lambda}_{eq}$ are interpolated from the expanded D20 suite. When interpolating over z_{re}, we correct for the I-front crossing time of the cell by averaging the opacity in the least and most recently ionized gas. For $\left.\frac{\partial\overline{\lambda}}{\partial\Gamma_{HI}}\right|_t$, we assume a power law $\overline{\lambda} \propto \Gamma_{HI}^\xi$, where $\xi = 2/3$. This form is motivated by McQuinn et al. (2011), the constraints of B21, as well as our D20-style calibration simulations. Equation (2) is integrated in fully ionized cells with $\Gamma_{-12} \geqslant 0.03$. In partially ionized cells or those with $\Gamma_{-12} < 0.03$, we set $\overline{\lambda} = \overline{\lambda}_{eq}$. Since $\overline{\lambda}$ depends on Γ_{-12}, we iterate Equations (1)–(2) until convergence. The D20-style simulations that we used to calibrate Equation (2) included up to $\times 100$ impulsive increases in Γ_{-12} as well as more realistic cases with gradual evolution. Equation (2) captures $\overline{\lambda}(t)$ in the gradually time-varying-Γ simulations to better than a few percent, while a straight interpolation overestimates it by 10%–15%. Our impulsive tests yielded similar levels of improvement. Consistent with the results of these tests, we use $t_{relax} = 100\,Myr$.

2.3. Density Fields and Source Models

The RT sims were run on a coarse-grained version of the $(200\,h^{-1}\,Mpc)^3$ hydrodynamics simulation in D'Aloisio et al. (2018), which employed a modified version of the code of Trac & Pen (2004). Density fields and halo catalogs were saved at time intervals of $10\,Myr$ from $z = 12 - 4.5$. The halo mass functions are converged down to $2 \times 10^{10}\,h^{-1}M_\odot$, more massive than the smallest halos believed to have contributed to reionization. We extended our sources by generating sub-resolution halos down to $M_{min} = 10^9\,h^{-1}M_\odot$ using the nonlinear biasing method of Ahn et al. (2015), applied with the halo mass function of Trac et al. (2015). (As discussed below, we have also run tests with $M_{min} = 10^8\,h^{-1}M_\odot$.) We used two models for the ionizing photon production rate of each halo: $\dot{n}_\gamma =$ constant (dependent only on z) and $\dot{n}_\gamma \propto$ UV luminosity (L_{UV}), where $\dot{n}_\gamma$ is the number of photons per unit time produced by a halo. The former is our fiducial model, which assigns more weight to low-mass galaxies in the ionizing photon budget. As we will see, the motivation for this choice is that the short value of λ_{912}^{mfp} ($z = 6$) favors models in which reionization is driven by faint, less-biased sources. For the L_{UV} model, we abundance matched to the UV luminosity function of Finkelstein et al. (2019). In both cases we chose the overall normalization of $\dot{n}_\gamma$ at each redshift to set the global emissivity history, $\dot{N}_\gamma(z)$. We varied $\dot{N}_\gamma(z)$ by trial and error to find reionization models consistent with the Planck τ_{CMB} constraints and the mean free path measurements.

3. Results

In Figure 1 we show four models chosen to illustrate our conclusions. In clockwise order, starting at the top left, the panels show the volume-weighted mean ionized fraction, comoving MFP at 1 Ry (λ_{912}^{mfp}), comoving ionizing emissivity ($\dot{N}_\gamma$), temperature at the cosmic mean density (T_0), volume-weighted mean Γ_{-12} in ionized gas, and the cumulative CMB optical depth. We compare against an assortment of existing
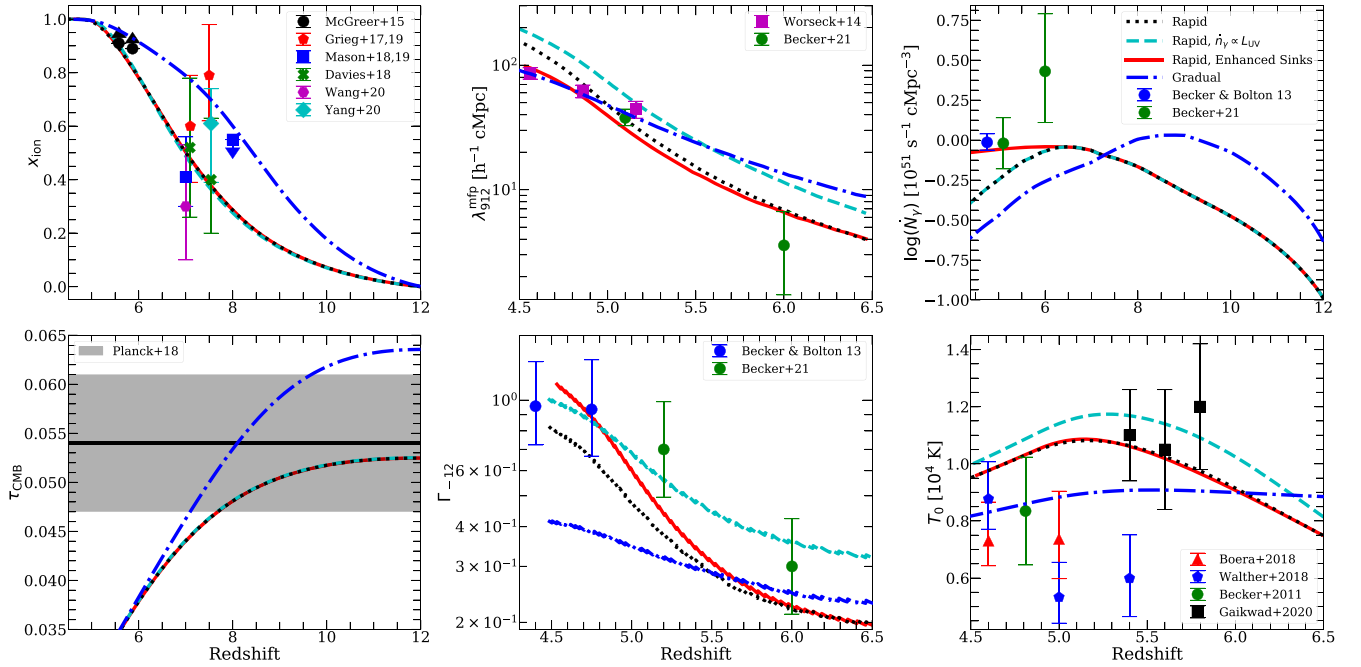
Figure 1. Reionization observables in our models. In clockwise order, starting from the top left, we show the ionized fraction, comoving MFP at 1 Ry, source comoving emissivity, IGM temperature at the cosmic mean density, H photoionization rate, and CMB optical depth. We compare against a selection of recent observational constraints with 1σ error bars (McGreer et al. 2015; Greig et al. 2016, 2019; Davies et al. 2018; Mason et al. 2018, 2019; Worsecket al. 2014; Planck Collaboration et al. 2020; Becker & Bolton 2013; Becker et al. 2011; Walther et al. 2019; Boera et al. 2019; Gaikwad et al. 2020; Wang et al. 2020; Yang et al. 2020).

constraints. To calculate $\lambda_{912}^{\rm mfp}$, we traced 50,000 sight lines from random locations, created mock quasar absorption spectra, and fit to the model of Prochaska et al. (2009) and Worseck et al. (2014).[1]

All models in Figure 1 end reionization at $z = 5.1$ and formally have the same duration of 780 Myr ($x_{\rm ion} = 1$–99%). The key distinction between the rapid and gradual scenarios is how quickly $x_{\rm ion}$ evolves in the last half of reionization. In the rapid model (black/dotted), the emissivity peaks at $z \approx 6.5$ and reionization proceeds rapidly after its $z = 7.1$ midpoint. As a result, Γ_{-12} and $\lambda_{912}^{\rm mfp}$ grow rapidly between $z = 6$ and 5.2, consistent with the measurements at those redshifts. The cyan/ dashed curve shows a model with the same emissivity, but with $\dot{n}_\gamma \propto L_{\rm UV}$. In this case reionization is driven by rarer, brighter galaxies[2] that, on average, produce larger Γ_{-12} in ionized bubbles. This results in $\lambda_{912}^{\rm mfp}$ being too long across all redshifts.

A principal conclusion from our modeling is that the short $\lambda_{912}^{\rm mfp}(z = 6)$ measured by B21 prefers faint, less-biased sources as the main drivers of reionization. We have run a set of models with a lower $M_{\rm min}$ of $10^8 \, h^{-1} \, M_\odot$. Adopting the same $\dot{N}_\gamma$ as in our rapid model, we find $\Gamma_{-12} = 0.2$ and $\lambda_{912}^{\rm mfp} = 5h^{-1}$ Mpc at $z = 6$. The dependence of $\lambda_{912}^{\rm mfp}$ on $M_{\rm min}$ can be understood in terms of halo bias. Sources are less clustered in models with

lower $M_{\rm min}$, which leads to ionized bubbles being smaller, on average. Large-scale fluctuations in $\Gamma_{\rm HI}$ are also reduced. In contrast, for models with highly clustered sources, the intense ionizing radiation in overdense regions quickly clears away the local sinks, allowing this radiation to penetrate much further into the IGM bulk.

In the gradual model (blue/dotted–dashed), reionization proceeds more gradually after its $z = 8.5$ midpoint. By $z = 6$, more of the gas has relaxed in response to photoheating. This, combined with the larger $x_{\rm ion}$, results in a factor of 1.5 longer $\lambda_{912}^{\rm mfp}$ at $z = 6$ compared to the rapid model. The evolution in Γ_{-12} is flatter but it undershoots by a factor of ~ 2 the measurements of Becker & Bolton (2013) at $z < 5$. Generally, models in which most of the IGM was reionized well before $z = 6$ are difficult to reconcile with a short $\lambda_{912}^{\rm mfp}(z = 6)$. We have confirmed this with other runs as well, including those with $M_{\rm min} = 10^8 h^{-1} M_\odot$. The problem is that the local $\lambda_{912}^{\rm mfp}$ grow with time after $z_{\rm re}$ owing to relaxation and photoevaporation. In gas that was reionized at higher redshift, the only way to obtain low $\lambda_{912}^{\rm mfp}$ is to lower Γ_{-12}. But the slow evolution results in undershooting the Lyα forest measurements of Γ_{-12} at $z \sim 5$. Hence, another principal conclusion from our modeling is that a rapidly evolving $x_{\rm ion}$ is required to recover both the short value of $\lambda_{912}^{\rm mfp}$ at $z = 6$ and its rapid evolution to $z = 5.2$. However, we note that the rapid models are in 2σ–3σ tension with the McGreer et al. (2015) constraints on $x_{\rm ion}$ (top left of Figure 1). Updating these constraints with more QSO sight lines will provide a critical test of our assertion.

There are two more obvious deficits of the rapid model (black/dashed): (1) the quick growth in $\lambda_{912}^{\rm mfp}$ continues below $z = 5.2$, which is incompatible with measurements; (2) relatedly, to control the growth of Γ_{-12} and $\lambda_{912}^{\rm mfp}$ at $z < 5.5$, $\dot{N}_\gamma$ must fall by $> 40\%$ in the 240 Myr between $z = 6$ and 5, a rapid evolution in the galaxy population (see, however, Ocvirk et al. 2021). We emphasize that $\dot{N}_\gamma(z)$ is an input to our

---

[1] Our sight lines do not start on QSOs, and thus are not affected by biases from the proximity effect (D'Aloisio et al. 2018; Becker et al. 2021). When we anchored sight lines on massive halos, we found that the model of Prochaska et al. (2009) did not provide a good fit at rest-frame 900 Å $\lesssim \lambda < 912$Å, owing to the local clustering of sources and the back-reaction of $\Gamma_{\rm HI}$ on $\lambda_{912}^{\rm mfp}$. Excluding these wavelengths in the fit gave the unbiased $\lambda_{912}^{\rm mfp}$. In this work, we assume that the observations represent the unbiased $\lambda_{912}^{\rm mfp}$. For reference, the biased $\lambda_{912}^{\rm mfp}(z = 6)$ is 9.3, 15.8, 15.1, 9.1 Mpc h^{-1} in the rapid, gradual, $\dot{n}_\gamma \propto L_{\rm UV}$, and enhanced sinks models, respectively.

[2] For the $\dot{n}_\gamma \propto L_{\rm UV}$ model, half the ionizing photons are produced by halos with $M < M_{1/2} = (0.39, 1.8, 3.4) \times 10^{10} h^{-1} M_\odot$ at $z = (9, 6, 5)$. For the model with $\dot{n}_\gamma$ independent of $L_{\rm UV}$, production is peaked around $M_{\rm min}$; we find $M_{1/2} = (1.6, 1.8, 1.8) \times 10^9 h^{-1} M_\odot$.

simulations; the decline is not the result of any feedback prescription. D20 found that their $\lambda_{912}^{\mathrm{mfp}}$ are converged in resolution at the 10% (factor of ~2) level in relaxed (unrelaxed gas), respectively. Moreover, up to $\Delta t \approx 10\,\mathrm{Myr}$ after z_{re}, D20 found $\lambda_{912}^{\mathrm{mfp}}$ similar to the unheated simulations of Emberson et al. (2013). This argues against numerical convergence being the sole culprit.

One plausible explanation for the behavior of $\dot{N}_\gamma$ is that our subgrid model overestimates $\lambda_{912}^{\mathrm{mfp}}$ in overdense cells, e.g., by inadequately sampling massive sinks near the end of reionization. To illustrate that we can obtain milder evolution in $\dot{N}_\gamma$ through sinks, we crudely scale down $\lambda_{912}^{\mathrm{mfp}}$ in all overdense cells after $z = 6.5$ by a factor of $[(1 + z)/(1 + 6.5)]^{3.5}$, such that $\lambda_{912}^{\mathrm{mfp}}$ is a factor of 2 shorter in those cells by $z = 5.2$. The result is the rapid+enhanced sinks model (red/solid), for which $\dot{N}_\gamma$ levels off after $z = 6.5$. In this case, the enhanced sinks regulate the growth of Γ_{-12} and $\lambda_{912}^{\mathrm{mfp}}$ so they do not outpace the measurements below $z = 5.2$. This obviates the need for a rapid decline in $\dot{N}_\gamma$, illustrating an approximate degeneracy between the emissivity and the sinks.[3]

The thick curves in the top panel of Figure 2 show the cumulative number of photons per hydrogen atom absorbed. The thin curves show the cumulative recombinations.[4] For reference, the vertical line corresponds to reionization's end. All our models require ≈ 3 photons/H atom to complete reionization. This is a factor of 1.5–2 more than in recent models of the ionizing emissivity.[5] Although more photons are absorbed earlier in the gradual model, the cumulative number is similar to the rapid models because much of the gas remains unrelaxed in the latter.
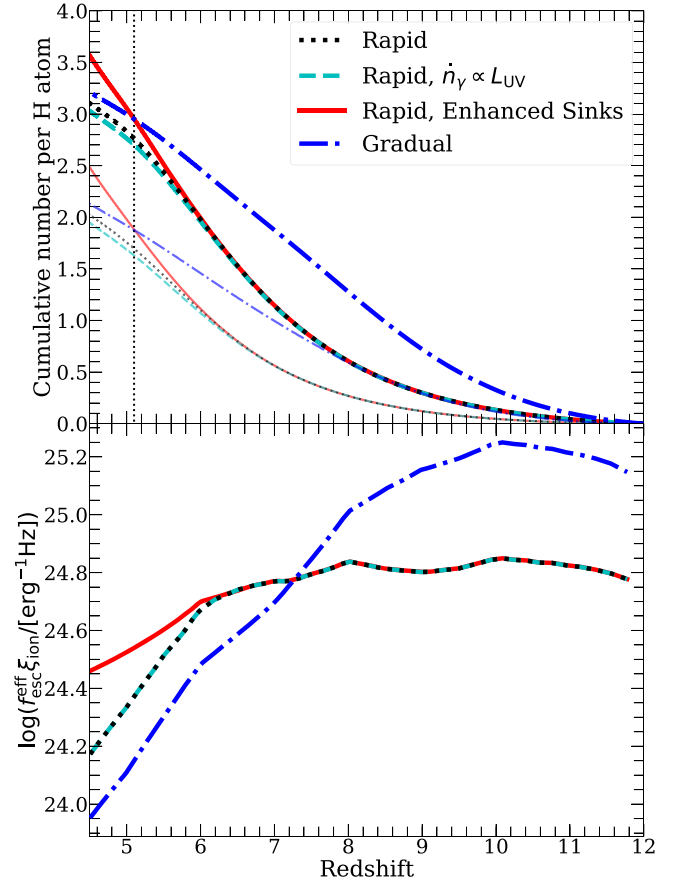
In a paper submitted concurrently with this work, Davies et al. (2021) quantify in detail the implications of the B21 measurement of $\lambda_{912}^{\mathrm{mfp}}(z = 6)$ for high-z galaxies. Considering also the dark pixel fraction constraints on $x_{\mathrm{ion}}(z = 5.9)$, they find that $6.1^{+1.1}_{-2.4}$ photons per baryon are required to bring reionization to 90% completion. Although this appears considerably larger than our budget, we note that $\lambda_{912}^{\mathrm{mfp}}(z = 6)$ in our rapid models are 1σ longer than the central value of B21, and the neutral fractions are $x_{\mathrm{HI}} = 20\%$. Adjusting for the former would bring down their budget to 3.7 photons per baryon. Adjusting for the latter would bring us further into agreement. Moreover, we have rerun the rapid simulation, but with a uniform $3.8 \times (2.5\times)$ boost to the clumping (emissivity). This yields $x_{\mathrm{ion}}(z = 5.9) = 88\%$ and $\lambda_{912}^{\mathrm{mfp}} = 3.65h^{-1}$, closer to the B21 central value of $3.57h^{-1}$ Mpc. It requires 5.2 photons/H atom by $z = 5.9$.

The emissivity is commonly modeled as $\dot{N}_\gamma = f_{\mathrm{esc}}^{\mathrm{eff}} \xi_{\mathrm{ion}} \rho_{\mathrm{UV}}$, where $f_{\mathrm{esc}}^{\mathrm{eff}}$ is an effective escape fraction, ξ_{ion} is the ionizing efficiency, and ρ_{UV} is the UV luminosity density. The bottom panel of Figure 2 shows the product, $f_{\mathrm{esc}}^{\mathrm{eff}} \xi_{\mathrm{ion}}$, obtained by applying this relation to our $\dot{N}_\gamma$ and integrating the UV luminosity function of Finkelstein et al. (2019) for

Figure 2. Top: cumulative number of absorptions (thick curves) and recombinations (thin faded curves) per H atom for our models. The vertical line corresponds to the end of reionization. Bottom: product of the effective LyC escape fraction and ionizing efficiency for each of our models. The rapid models are broadly consistent with observational constraints on ξ_{ion} provided that $f_{\mathrm{esc}}^{\mathrm{eff}} = 10\%$–40% (see the text).

ρ_{UV}. Previous studies have assumed $\log(\xi_{\mathrm{ion}}/[\mathrm{erg}^{-1}\mathrm{Hz}]) = 25.2$–25.3, consistent with the constraints of Bouwens et al. (2016) for $4 < z < 5$ galaxies. There is evidence that the bluest galaxies at higher redshift exhibit higher efficiencies, $\log(\xi_{\mathrm{ion}}/[\mathrm{erg}^{-1}\mathrm{Hz}]) = 25.6$–25.9 (Bouwens et al. 2016; Stark et al. 2017; Endsley et al. 2021). For the rapid models to be consistent with values of 25.8 (25.3) requires $f_{\mathrm{esc}}^{\mathrm{eff}} = 11(35)\%$. The gradual model requires a more extreme $f_{\mathrm{esc}}^{\mathrm{eff}} = 28(89)\%$ at its peak of $z = 10$. However, if we let $M_{\mathrm{min}} = 10^8\,h^{-1}M_\odot$, we find $f_{\mathrm{esc}}^{\mathrm{eff}} = 10(32)\%$, indicating that such an early peak in emissivity would likely require efficient star formation in galaxies with $M < 10^9\,h^{-1}M_\odot$ (see, e.g., Finkelstein et al. 2019). Our $f_{\mathrm{esc}}^{\mathrm{eff}}$ are similar to those reported by Davies et al. (2021). That our rapid models require $f_{\mathrm{esc}}^{\mathrm{eff}} = 10\%$–40% supports the conclusion that faint $z > 6$ galaxies must have been prolific leakers of LyC radiation, if reionization was driven by stellar emissions.

The top and bottom sets of panels in Figure 3 show light cones through our rapid+enhanced sinks and gradual models, respectively. In each set, the top(bottom) panel shows $\Gamma_{-12}(\lambda_{912}^{\mathrm{mfp}})$. The neutral islands down to $z \approx 5.5$ likely make both models compatible with the large opacity fluctuations observed in the Lyα forest (Kulkarni et al. 2019; Nasir & D'Aloisio 2020). The Lyα forest mean flux evolution, however,

---

[3] We have also run an enhanced sinks version of the gradual model. While it is in better agreement with the $z < 5$ Γ_{-12} measurements—reconciling a major deficiency of the model—we find $\lambda_{912}^{\mathrm{mfp}}(z = 6) = 14h^{-1}$ Mpc. This is still much larger than the measurement, suggesting that an even larger boost to the sinks at $z \sim 6$ would be required in this scenario.

[4] The number of recombinations is given by the total number of absorptions minus the net number of ionizations.
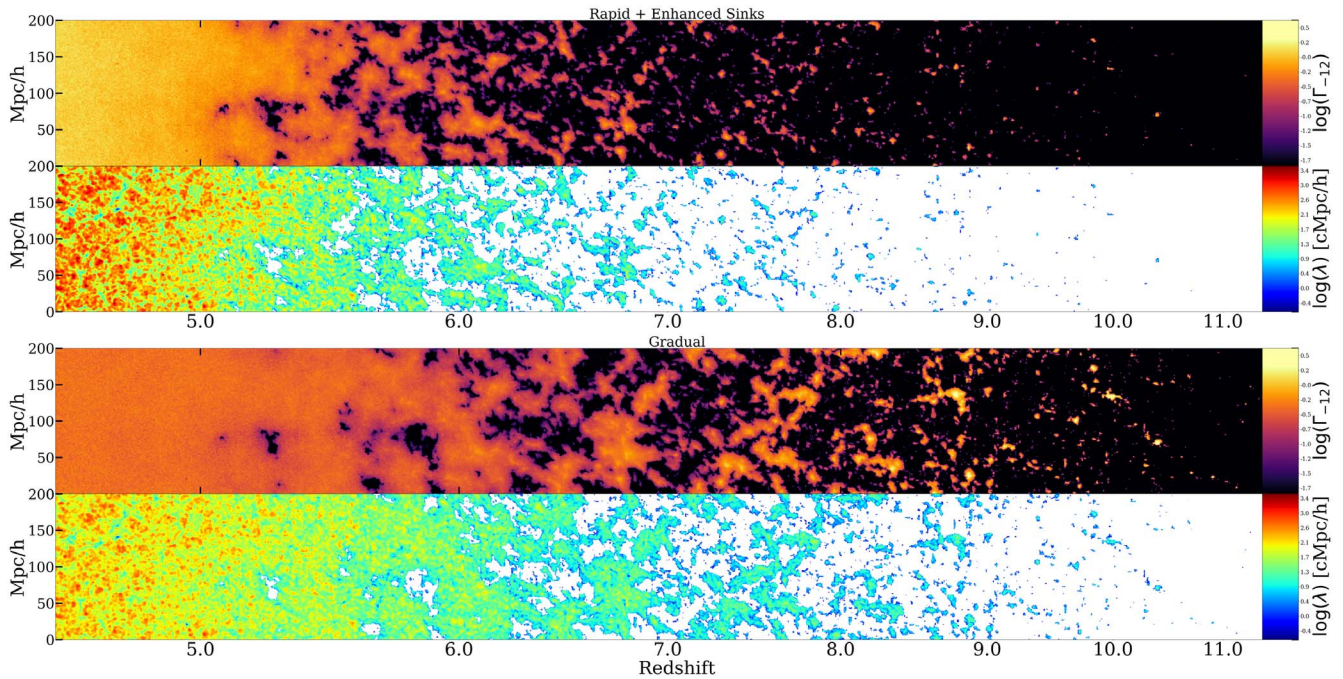
[5] We find 1.5 and 1.8 photons/H atom in the models of Robertson et al. (2015) and Finkelstein et al. (2019), respectively.

Figure 3. Light-cone slices (1 Mpc h^{-1} thick) of Γ_{-12} and $\lambda_{912}^{\mathrm{mfp}}$ from our rapid+enhanced sinks (top) and gradual (bottom) models. In the rapid model, $\lambda_{912}^{\mathrm{mfp}}$ evolves quickly at $z < 6$ as the gas relaxes and neutral islands disappear. After reionization is finished, $\lambda_{912}^{\mathrm{mfp}}$ is limited by sinks in overdense regions. In the gradual model most gas is relaxed by $z \sim 6$ and there is less neutral gas, resulting in a longer $\lambda_{912}^{\mathrm{mfp}}$.

may already disfavor the gradual model (see bottom-middle of Figure 1). Another contrasting feature is the existence of large ($R \sim$ 10s Mpc) ionized bubbles out to $z \sim 9$ in the gradual model, which is of interest for recent observations of bright LAE overdensities at $z > 7$ (Castellano et al. 2018; Tilvi et al. 2020; Endsley et al. 2021). The different global x_{ion} and morphologies may be testable by forthcoming 21 cm surveys.

4. Conclusion

We have explored the implications of the B21 MFP measurements for reionization. Taken together with constraints on the intensity of the metagalactic ionizing background, we have argued that the rapid evolution from $\lambda_{\mathrm{mfp}}^{912}(z = 6) = 3.57_{-2.14}^{+3.09}$ cMpc h^{-1} to $\lambda_{\mathrm{mfp}}^{912}(z = 5.1) = 37.71_{-5.06}^{+6.72}$ cMpc h^{-1} favors a rapid and late reionization process. We have also argued that the short value of $\lambda_{\mathrm{mfp}}^{912}(z = 6)$ is evidence that reionization was driven primarily by the faintest, least biased galaxies among its sources. In our preferred models, ≈ 3 ionizing photons/H atom are required to complete reionization. Half of them come from galaxies with $M \sim 10^9 h^{-1} M_\odot$, or lower. At $z = 6(8)$, this corresponds to UV magnitudes $M_{1600} \gtrsim -12.9(-14.0)$. In addition to confirming the low value of $\lambda_{\mathrm{mfp}}^{912}(z = 6)$, other avenues forward include updating the Lyα forest dark pixel limits on x_{ion} and constraining the IGM temperature at $z \sim 5.5$. Our analysis highlights the complementary channels for constraining reionization with QSO absorption spectra.

ORCID iDs

Christopher Cain ⓘ https://orcid.org/0000-0001-9420-7384
George D. Becker ⓘ https://orcid.org/0000-0003-2344-263X

References

Abel, T., & Wandelt, B. D. 2002, MNRAS, 330, L53
Ahn, K., Iliev, I. T., Shapiro, P. R., & Srisawat, C. 2015, MNRAS, 450, 1486
Becker, G. D., & Bolton, J. S. 2013, MNRAS, 436, 1023
Becker, G. D., Bolton, J. S., Haehnelt, M. G., & Sargent, W. L. W. 2011, MNRAS, 410, 1096
Becker, G. D., Bolton, J. S., Madau, P., et al. 2015, MNRAS, 447, 3402
Becker, G. D., D'Aloisio, A., Christenson, H. M., et al. 2021, arXiv:2103.16610
Boera, E., Becker, G. D., Bolton, J. S., & Nasir, F. 2019, ApJ, 872, 101
Bosman, S. E. I., Fan, X., Jiang, L., et al. 2018, MNRAS, 479, 1055
Bouwens, R. J., Smit, R., Labbé, I., et al. 2016, ApJ, 831, 176
Castellano, M., Pentericci, L., Vanzella, E., et al. 2018, ApJL, 863, L3
D'Aloisio, A., McQuinn, M., Davies, F. B., & Furlanetto, S. R. 2018, MNRAS, 473, 560
D'Aloisio, A., McQuinn, M., Maupin, O., et al. 2019, ApJ, 874, 154
D'Aloisio, A., McQuinn, M., Trac, H., Cain, C., & Mesinger, A. 2020, ApJ, 898, 149
Davies, F., Bosman, S., Furlanetto, S., Becker, G. D., & D'Aloisio, A. 2021, arXiv:2105.10518
Davies, F. B., Hennawi, J. F., Bañados, E., et al. 2018, ApJ, 864, 142
Eilers, A.-C., Davies, F. B., & Hennawi, J. F. 2018, ApJ, 864, 53
Emberson, J. D., Thomas, R. M., & Alvarez, M. A. 2013, ApJ, 763, 146
Endsley, R., Stark, D. P., Charlot, S., et al. 2021, MNRAS, 502, 6044
Finkelstein, S. L., D'Aloisio, A., Paardekooper, J.-P., et al. 2019, ApJ, 879, 36
Gaikwad, P., Rauch, M., Haehnelt, M. G., et al. 2020, MNRAS, 494, 5091
Greig, B., Mesinger, A., & Bañados, E. 2019, MNRAS, 484, 5094
Greig, B., Mesinger, A., Haiman, Z., & Simcoe, R. A. 2016, MNRAS, 466, 4239

Iliev, I. T., Mellema, G., Ahn, K., et al. 2014, MNRAS, 439, 725
Kashikawa, N., Shimasaku, K., Malkan, M. A., et al. 2006, ApJ, 648, 7
Keating, L. C., Kulkarni, G., Haehnelt, M. G., Chardin, J., & Aubert, D. 2020a, MNRAS, 497, 906
Keating, L. C., Weinberger, L. H., Kulkarni, G., et al. 2020b, MNRAS, 491, 1736
Kulkarni, G., Keating, L. C., Haehnelt, M. G., et al. 2019, MNRAS, 485, L24
Mason, C. A., Fontana, A., Treu, T., et al. 2019, MNRAS, 485, 3947
Mason, C. A., Treu, T., de Barros, S., et al. 2018, ApJL, 857, L11
McGreer, I. D., Mesinger, A., & D'Odorico, V. 2015, MNRAS, 447, 499
McQuinn, M., Oh, S. P., & Faucher-Giguère, C.-A. 2011, ApJ, 743, 82
Nasir, F., & D'Aloisio, A. 2020, MNRAS, 494, 3080
Ocvirk, P., Lewis, J. S. W., Gillet, N., et al. 2021, arXiv:2105.01663
Ono, Y., Ouchi, M., Mobasher, B., et al. 2011, ApJ, 744, 83
Park, H., Shapiro, P. R., Choi, J.-H., et al. 2016, ApJ, 831, 86
Pentericci, L., Vanzella, E., Fontana, A., et al. 2014, ApJ, 793, 113
Planck Collaboration, Aghanim, N., Akrami, Y., et al. 2020, A&A, 641, A6

Prochaska, J. X., Worseck, G., & O'Meara, J. M. 2009, ApJL, 705, L113
Qin, Y., Mesinger, A., Bosman, S. E. I., & Viel, M. 2021, MNRAS, 506, 2390
Robertson, B. E., Ellis, R. S., Furlanetto, S. R., & Dunlop, J. S. 2015, ApJL, 802, L19
Schenker, M. A., Stark, D. P., Ellis, R. S., et al. 2012, ApJ, 744, 179
Stark, D. P., Ellis, R. S., Charlot, S., et al. 2017, MNRAS, 464, 469
Tilvi, V., Malhotra, S., Rhoads, J. E., et al. 2020, ApJL, 891, L10
Trac, H., & Cen, R. 2007, ApJ, 671, 1
Trac, H., Cen, R., & Mansfield, P. 2015, ApJ, 813, 54
Trac, H., & Pen, U.-L. 2004, NewA, 9, 443
Walther, M., Oñorbe, J., Hennawi, J. F., & Lukić, Z. 2019, ApJ, 872, 13
Wang, F., Davies, F. B., Yang, J., et al. 2020, ApJ, 896, 23
Worseck, G., Prochaska, J. X., O'Meara, J. M., et al. 2014, MNRAS, 445, 1745
Wu, X., McQuinn, M., & Eisenstein, D. 2021, JCAP, 2021, 042
Yang, J., Wang, F., Fan, X., et al. 2020, ApJL, 897, L14